

Generalized cluster algorithms for Potts lattice gauge theory

Anthony E. Pizzimenti
George Mason University
apizzime@gmu.edu

Paul Duncan
Indiana University
pauldunc@iu.edu

Benjamin Schweinhart
George Mason University
bschwei@gmu.edu

July 21, 2025

Abstract

Monte Carlo algorithms, like the *Swendsen–Wang* and *invaded-cluster*, sample the Ising and Potts models asymptotically faster than single-spin Glauber dynamics do. Here, we generalize both algorithms to sample *Potts lattice gauge theory* by way of a 2-dimensional cellular representation called the *plaquette random-cluster model*. The invaded-cluster algorithm targets Potts lattice gauge theory at criticality by implementing a stopping condition defined in terms of *homological percolation*, the emergence of spanning surfaces on the torus. Simulations for \mathbb{Z}_2 and \mathbb{Z}_3 lattice gauge theories on the cubical 4-dimensional torus indicate that both generalized algorithms exhibit much faster autocorrelation decay than single-spin dynamics and allow for efficient sampling on 4-dimensional tori of linear scale at least 40.

1 Introduction

The q -state *Potts lattice gauge theory* (PLGT) on a finite subcomplex X of the cubical complex \mathbb{Z}^d is a random assignment of spins in \mathbb{Z}_q to the edges of X . These assignments are induced by the Hamiltonian

$$\mathbf{H}(f) = - \sum_{x \in X} \mathbf{1}_{\delta^1 f(x)=0},$$

where $x \in X$ is a *plaquette* (2-dimensional cell) and $\delta^1 f(x)$ is the oriented sum (mod q) of spins on the edges incident to x [26, 33]. Recent work in [12, 24, 31] generalizes the Fortuin–Kastelyn *random-cluster model* (a graphical representation of the Potts model) to construct a 2-dimensional cellular representation of Potts lattice gauge theory called the *plaquette random-cluster model* (PRCM) [17]. We use this cellular representation to define non-local Monte Carlo algorithms for Potts lattice gauge theory. Specifically, we generalize the *Swendsen–Wang* [32] and *invaded-cluster* algorithms [27, 28], procedures that revolutionized computational simulations of the Potts model. Both algorithms alternate between sampling 2-subcomplexes and sampling spins: the former does so according to the PRCM and PLGT;¹ the latter builds a 2-complex cell-by-cell until a stopping condition based on *homological percolation* — the emergence of “giant surfaces”

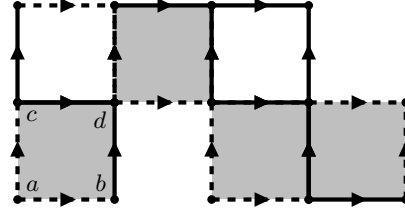


Figure 1: A cubical complex with fourteen 0-cells (vertices), nineteen 1-cells (edges), and four 2-cells (filled squares). Edge coefficients are 0 (solid) or 1 (dashed).

— is met, then re-samples spins and begins anew.

In Section 2, we define Potts lattice gauge theory, the plaquette random-cluster model, and the coupling between them. Section 3 covers the Swendsen–Wang and invaded-cluster algorithms, including a proof that the former has the correct stationary distribution. We then discuss consequences of the duality properties of the PRCM in Section 4; the Loop–Cluster coupling [34] and its generalization [22] are recovered by considering the behavior of the coupling between Potts (hyper)lattice gauge theory and the plaquette random cluster model under the latter’s duality transformation. In Section 5, we conclude by describing practical implementations of the Swendsen–Wang and invaded-cluster algorithms and analyzing autocorrelation decay in computational simulations.

2 Background and definitions

A *finite cubical complex* X is a combinatorial object made up of vertices, edges, and *plaquettes* (squares). Typically, X is a finite subset of \mathbb{Z}^d , the tiling of \mathbb{R}^d by unit d -cubes with corners at integer coordinates. Elements of \mathbb{Z}^d are i -cells, where i indicates dimension: 0-cells are vertices of the integer lattice, 1-cells are edges in the nearest-neighbors graph on the vertices, and 2-cells the (square) minimal cycles formed by the edges. In this context, “2-cells,” “plaquettes,” and “2-plaquettes” are the same. We are mostly interested in cells of dimension less than 3 (though 3-cells enter into the definition of the plaquette invaded-cluster algorithm). To impose periodic boundary conditions on finite complexes, we “glue” opposite cells of $[0, N]^d \subset \mathbb{Z}^d$ together to form the *scale- N d -fold cubical torus* \mathbb{T}_N^d . See Figure 1 for an illustration.

¹ An algorithm of this form was previously described for the special case $q = 2$ in [4, 7].

2.1 Potts lattice gauge theory

The q -state Potts lattice gauge theory (PLGT) on a cubical complex X assigns spins in \mathbb{Z}_q to the edges of X .² As our techniques are inspired by algebraic topology, we assume its vocabulary and refer to the state space of Potts lattice gauge theory as the group of 1-cochains, denoted by $C^1(X; \mathbb{Z}_q)$. Each $f \in C^1(X; \mathbb{Z}_q)$ is a function that assigns a spin to each edge of X so that the sign of the spin flips whenever its corresponding edge's orientation is reversed. When q is prime, $C^1(X; \mathbb{Z}_q)$ is a \mathbb{Z}_q -vector space.³

The *coboundary* (or *discrete exterior derivative*) of a 1-cochain is a 2-cochain — a map assigning \mathbb{Z}_q spins to plaquettes — and belongs to the group $C^2(X; \mathbb{Z}_q)$ of 2-cochains on X . For $f \in C^1(X; \mathbb{Z}_q)$ and a plaquette x , the coboundary $\delta^1 f$ assigns to x the oriented sum of the spins on its bounding edges. The plaquette $x = \{abcd\}$ in Figure 1, for example, is oriented so that its boundary is

$$\partial_2(x) = \{ab\} - \{ac\} + \{bd\} - \{cd\}$$

and, extending linearly, we define $\delta^1 f(x)$ by

$$\begin{aligned} (\delta^1 f)(x) &= f(\{ab\}) - f(\{ac\}) + f(\{bd\}) - f(\{cd\}) \\ &= f(\partial_2(x)). \end{aligned}$$

We can also take the coboundary of a 0-cochain $g \in C^0(X; \mathbb{Z}_q)$, an assignment of spins to the vertices of X . If e is an oriented edge from v to w , then $\delta^0 g(e) = g(w) - g(v)$. As $\delta^1 \circ \delta^0 = 0$, the Hamiltonian is unchanged by the addition of the coboundary of a 0-cochain: this is the action of gauge transformations on $C^1(X; \mathbb{Z}_q)$. See Appendix A.1 for complete definitions.

The q -state Potts lattice gauge theory ν on X with inverse temperature β is then the Gibbs distribution on $C^1(X; \mathbb{Z}_q)$ induced by the Hamiltonian \mathbf{H} that counts the number of non-frustrated plaquettes $x \in X$ (i.e. plaquettes x such that $\delta^1 f(x) = 0$) [26, 33] given by

$$\mathbf{H}(f) = - \sum_{x \in X} \mathbf{1}_{\delta^1 f(x)=0}.$$

In all, PLGT has law

$$\nu(f) = \frac{1}{Z(q, \beta)} e^{-\beta \mathbf{H}(f)},$$

² Counter to tradition, it is convenient for us to identify $\mathbb{Z}_q := \{0, 1, \dots, q-1\}$ with the group of integers modulo q rather than the q^{th} complex roots of unity.

³ Cochains in $C^1(X; \mathbb{Z}_q)$ are sometimes referred to as *discrete differential forms*, as they play the same role in cubical cohomology theory as differential forms do in de Rham cohomology.

assigning the probability $\nu(f)$ to the edge spin assignment f . We can extend this model to define a random i -cochain in $C^i(X; \mathbb{Z}_q)$, where the case $i = 0$ is the classical q -state Potts model [24, 33].

Potts lattice gauge theory has been studied as a relatively simple discrete example of a model with a gauge symmetry: when $q = 2$ or $q = 3$, it coincides with $\mathbb{Z}(q)$ *Euclidean lattice gauge theory* (with $\mathbb{Z}(q)$ the complex q^{th} roots of unity). In addition, *Ising lattice gauge theory* — the case $q = 2$ — has met renewed interest because of its relationship with the *toric code* [1], spurring on development of fast-converging algorithms for sampling these models.

2.2 Plaquette random-cluster model

To divine the *plaquette random-cluster model*, we use the same strategy as for the random-cluster model: expand and manipulate the partition function of its corresponding Potts model. For motivational purposes, we first derive the classical random-cluster model. If G is a finite graph with vertices V_G and edges E_G , $C^0(G; \mathbb{Z}_q)$ is the set of spin assignments $f : V_G \rightarrow \mathbb{Z}_q$. Given a subgraph $H \subset G$, an assignment f is *compatible* with H whenever $f(u) = f(w)$ for all edges (v, w) in H ; call the set of all compatible spin assignments $Z^0(H; \mathbb{Z}_q)$. With β an inverse temperature parameter, $p = 1 - e^{-\beta}$, and F the event that $f(v) = f(w)$,

$$\begin{aligned} e^{\beta \mathbf{1}_F} &= e^\beta ((1 - e^{-\beta}) \mathbf{1}_F + e^{-\beta}) \\ &= e^\beta (p \mathbf{1}_F + (1 - p)) \end{aligned}$$

for fixed f . Noticing that

$$\sum_f e^{-\beta \mathbf{H}(f)} = \sum_f \prod_{(v,w)} e^{\beta \mathbf{1}_F},$$

the partition function $Z := Z(q, \beta)$ for the Potts model on G is given by

$$\begin{aligned} Z &= \sum_f \prod_{(v,w)} e^\beta (p \mathbf{1}_F + (1 - p)) \\ &= e^{\beta |E_G|} \left[\sum_{H \subset G} p^{|E_H|} (1 - p)^{|E_G| - |E_H|} |Z^0(H; \mathbb{Z}_q)| \right]. \end{aligned}$$

Spin assignments are compatible with H exactly when they are constant the connected components of H , so $|Z^0(H; \mathbb{Z}_q)|$ equals $q^{\mathbf{b}_0(H)}$, where $\mathbf{b}_0(H)$ denotes the number of components. As we will see later, this equals the size of the zero-dimensional homology group $H_0(H, \mathbb{Z}_q)$. The *random-cluster model* assigns H probability proportional to

$$p^{|E_H|} (1 - p)^{|E_G| - |E_H|} q^{\mathbf{b}_0(H)},$$

with partition function $\mathcal{Z}(p, q) = e^{-\beta |E_G|} Z(q, \beta)$ [19].

In the *plaquette random-cluster model* we swap the Potts model for PLGT, upgrading dimension as needed. Given a finite cubical complex X with vertices V_X , edges E_X , and plaquettes U_X , a *percolation subcomplex* P is a subcomplex of X where we require $V_P = V_X$, $E_P = E_X$, and $U_P \subset U_X$. A spin assignment $f \in C^1(X; \mathbb{Z}_q)$ is *compatible* with P when, for all plaquettes $x \in U_P$, the oriented sum of spins on the edges of x is zero (mod q) — equivalently, when $\delta^1 f(x) = 0$. Like before, the set of compatible assignments is written as $Z^1(P; \mathbb{Z}_q)$. Using the same trick, the partition function $Z := Z(q, \beta)$ for Potts lattice gauge theory is

$$\begin{aligned} Z &= \sum_f \prod_x e^{\beta} (p \mathbf{1}_F + (1-p)) \\ &= e^{\beta |U_X|} \left[\sum_{P \subset X} p^{|U_P|} (1-p)^{|U_X| - |U_P|} |Z^1(P; \mathbb{Z}_q)| \right], \end{aligned}$$

where F is the event that $\delta^1 f(x) = 0$.

Here, there is a key difference from the 0-dimensional case: we can no longer express the number of compatible spin assignments as a power of q . Before explaining why, we account for the action of the gauge transformation on $C^1(X; \mathbb{Z}_q)$. Any vertex spin assignment $g \in C^0(X; \mathbb{Z}_q)$ gives rise to an edge spin assignment $\delta^0 g \in C^1(X; \mathbb{Z}_q)$. As consequences of the identity $\delta^1 \circ \delta^0 = 0$, we have that $g \in Z^1(P; \mathbb{Z}_q)$ for any P , and the Hamiltonian \mathbf{H} of PLGT remains invariant under the transformation $f \mapsto f + \delta^0 g$. The group of 1-coboundaries $B^1(P; \mathbb{Z}_q)$ is the collection of cocycles $\delta^0 g$; importantly, these do not depend on P . The quotient group

$$H^1(P; \mathbb{Z}_q) := Z^1(P; \mathbb{Z}_q) / B^1(P; \mathbb{Z}_q)$$

of cocycles modulo coboundaries is the *cohomology* of P . By Lagrange's theorem on quotient groups,

$$\begin{aligned} |Z^1(P; \mathbb{Z}_q)| &= |H^1(P; \mathbb{Z}_q)| |B^1(P; \mathbb{Z}_q)| \\ &= |H^1(P; \mathbb{Z}_q)| |B^1(X; \mathbb{Z}_q)|. \end{aligned}$$

Abbreviating $B^1(X; \mathbb{Z}_q)$ and $H^1(P; \mathbb{Z}_q)$ to B_q^1 and H_q^1 respectively, we can rewrite $Z := Z(q, \beta)$ as

$$e^{\beta |U_X|} |B_q^1| \left[\sum_{P \subset X} p^{|U_P|} (1-p)^{|U_X| - |U_P|} |H_q^1| \right].$$

The *plaquette random-cluster model* (PRCM) μ with parameters $p = 1 - e^{-\beta}$ and q assigns the percolation subcomplex $P \subset X$ probability

$$\mu(P) = \frac{1}{\mathcal{Z}(p, q)} p^{|U_P|} (1-p)^{|U_X| - |U_P|} |H^1(P; \mathbb{Z}_q)|,$$

as the $|B^1(X; \mathbb{Z}_q)|$ terms cancel. Akin to 0-dimensional case, $\mathcal{Z}(p, q) = e^{-\beta |U_X|} Z(q, \beta)$.

Hiraoka and Shirai introduced the prime- q case of the PRCM in the context of a mean-field analogue of this model, but did not connect their work to the literature on Potts lattice gauge theory [24]. Duncan and Schweinhart further studied the PRCM on \mathbb{Z}^d in [14], and the extension to general q was independently discovered by Duncan and Schweinhart [12, 13] and Shklarov [31]. Earlier attempts at this construction [18, 29] fell short [2] because they implicitly assumed that $|H^1(P; \mathbb{Z}_q)|$ always equals $q^{\text{rank } H^1(P; \mathbb{Z}_q)}$, but — even when q is prime — $|H^1(P; \mathbb{Z}_q)|$ depends on q . While $|H^1(P; \mathbb{Z}_q)| = q^{\text{rank } H^1(P; \mathbb{Z}_q)}$ holds true for subcomplexes of \mathbb{Z}^3 , it fails in higher dimensions and subcomplexes of the 4-torus. If $P \subset \mathbb{Z}^4$ is an embedding of the real projective plane, for example, $|H^1(P; \mathbb{Z}_2)| = 2$ but $|H^1(P; \mathbb{Z}_q)| = 0$ for odd q . By contrast, the 0-dimensional cohomology $|H^0(P; \mathbb{Z}_q)|$ always equals $q^{\text{bo}(P)}$. See [2] for a complete discussion of this phenomenon.

2.3 Coupling

Following Edwards and Sokal [16], we couple Potts lattice gauge theory ν (with parameters β and q) to the PRCM μ (with parameters $p = 1 - e^{-\beta}$ and q) as the joint distribution \mathcal{K} assigning probability

$$\mathcal{K}(f, P) \propto \prod_{x \in X} [(1-p)(\mathbf{1}_A) + p(\mathbf{1}_B)]$$

to each pairing of edge spin assignment $f \in C^1(X; \mathbb{Z}_q)$ and percolation subcomplex $P \subset X$. The product is taken over the plaquettes x of X ; A is the event that $x \notin P$, and B the event that $x \in P$ and $\delta^1 f(x) = 0$. The coupling is illustrated (in an algorithmic context) in Figure 2. Based on work by Hiraoka and Shirai in [24], Duncan and Schweinhart prove the following as Proposition 12 and Corollary 13 in [12]:

Proposition 1 (Marginals of \mathcal{K} , Prop. 12 in [12]). *The marginal distribution $\mathcal{K}(f, -)$ on f is Potts lattice gauge theory, and the marginal distribution $\mathcal{K}(-, P)$ on P is the plaquette random-cluster measure.*

Proposition 2 (Conditionals of \mathcal{K} , Cor. 13 in [12]). *The conditional distribution $\mathcal{K}(- | f)$ on percolation subcomplexes P given a cochain f is independent percolation with probability p over non-frustrated plaquettes in X . The conditional distribution $\mathcal{K}(- | P)$ on cochains f given a percolation subcomplex P is the uniform measure on $Z^1(P; \mathbb{Z}_q) = \ker \delta^1$, the group of cocycles of P .*

3 Cluster algorithms for PLGT

Using the coupling, we can generalize the *Swendsen–Wang algorithm* [32]. Given parameters $p = 1 - e^{-\beta}$ and $q \in \mathbb{Z}_{\geq 2}$, the following procedure takes as input the spin assignment $f_t \in C^1(X; \mathbb{Z}_q)$ at time t , and outputs an updated cochain f_{t+1} after passing through a percolation subcomplex P_{t+1} . As we prove below, the sample distributions for f_t and P_t converge to PLGT and the PRCM, respectively.

Algorithm 1 (*Plaquette Swendsen–Wang*).

- (1) For each plaquette $x \in X$, sample α uniformly over $[0, 1]$ and set

$$\omega_{t+1}(x) := \begin{cases} 0 & \delta^1 f_t(x) \neq 0 \\ \begin{cases} 1 & \alpha < p \\ 0 & \alpha \geq p \end{cases} & \delta^1 f_t(x) = 0 \end{cases}$$

- (2) Let P_{t+1} comprise all vertices and edges of X , and all plaquettes x where $\omega_{t+1}(x) = 1$.
- (3) Uniformly sample f_{t+1} from $Z^1(P_{t+1}; \mathbb{Z}_q)$, and set $t := t + 1$.
- (4) Return to (1) unless a suitable convergence threshold is met.

Lemma 3. *Because the Markov chain \mathbf{M} simulated by the plaquette Swendsen–Wang algorithm (Algorithm 1) is irreducible and aperiodic, it has a unique stationary distribution.*

Lemma 3 immediately implies the following theorem.

Theorem 4. *The q -state Potts lattice gauge theory ν is a reversible distribution for \mathbf{M} , and so is the unique stationary distribution for \mathbf{M} .*

Proof. Let f and f^* be cochains. Algorithm 1 tells us that the probability $\mathbf{P}(f \rightarrow f^*)$ of sampling f^* given f is the product of the conditional distributions in Proposition 2. With Proposition 1’s assertion that $\mathcal{K}(f, -) = \nu(f)$, we can say that

$$\nu(f) \mathbf{P}(f \rightarrow f^*) = \mathcal{K}(f, -) \sum_P \mathcal{K}(f^* | P) \mathcal{K}(P | f)$$

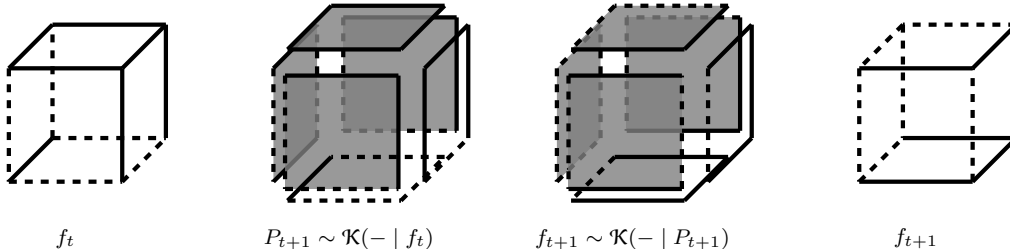


Figure 2: The plaquette Swendsen–Wang algorithm at work for $q = 2$; edge coefficients are 0 (solid) or 1 (dashed). Given some initial cochain f_t , the algorithm first samples P_{t+1} conditioned on f_t , then f_{t+1} conditioned on P_{t+1} . The figure also illustrates the coupled measure \mathcal{K} on the space of cochains and subcomplexes.

$$\begin{aligned} &= \sum_P \mathcal{K}(f, -) \frac{\mathcal{K}(f^*, P) \mathcal{K}(f, P)}{\mathcal{K}(-, P) \mathcal{K}(f, -)} \\ &= \sum_P \mathcal{K}(f^*, -) \frac{\mathcal{K}(f, P) \mathcal{K}(f^*, P)}{\mathcal{K}(-, P) \mathcal{K}(f^*, -)} \\ &= \mathcal{K}(f^*, -) \sum_P \mathcal{K}(f | P) \mathcal{K}(P | f^*) \\ &= \nu(f^*) \mathbf{P}(f^* \rightarrow f), \end{aligned}$$

so ν is a reversible — and thus stationary — distribution for \mathbf{M} . By Lemma 3, Potts lattice gauge theory is the unique stationary distribution for \mathbf{M} . \square

We can also describe an invasion percolation-type algorithm that relies on *homological percolation*, a generalization of crossing events in bond percolation [5, 6, 13]. Given a subcomplex P of the torus \mathbb{T}_N^d , homological percolation is the event that P contains a *giant cycle*, an i -chain that “wraps around” or “spans” the system (in the sense that it is non-trivial in the homology of the torus) [5]. When $i = 1$, the homological percolation event marks the emergence of a periodic path, an event used by Machta et al. [27, 28] as a “topological stopping rule” for the graphical invaded-cluster algorithm that samples the Potts model on the 2-torus.

Motivated by the following result [14], the *plaquette invaded-cluster algorithm* (Algorithm 2) generalizes the invaded-cluster algorithm in [28] to PLGT.

Theorem 5 (Duncan and Schweinhart). *Let P be distributed as the d -dimensional PRCM on \mathbb{T}_N^{2d} with parameters p and $q \geq 1$, and \mathbb{F} a field of characteristic not equal to 2. If R and S are the events that P contains no non-trivial giant cycles in $H_d(\mathbb{T}_N^{2d}; \mathbb{F})^4$ and that P contains giant cycles that form a basis for $H_d(\mathbb{T}_N^{2d}; \mathbb{F})$, respectively, then*

$$\begin{aligned} \mu(R) &\longrightarrow 0 & p < p_{\text{sd}} \\ \mu(S) &\longrightarrow 1 & p > p_{\text{sd}} \end{aligned}$$

as $N \rightarrow \infty$, where $p_{\text{sd}} = \sqrt{q}/(1 + \sqrt{q})$.

⁴ \mathbb{F} does not need to match \mathbb{Z}_q .

Here, p_{sd} corresponds to the *self-dual point* of PLGT under the transformation $\beta \mapsto 1 - e^{-\beta}$, conjectured to be the critical point for Potts lattice gauge theory in four dimensions [26]. Moreover, for any q , the homological percolation threshold for the PRCM on \mathbb{Z}^3 coincides with the area law–perimeter law transition for Wilson loop variables in the corresponding PLGT (assuming a widely believed conjecture on the regularity of the supercritical phase of the random-cluster model).⁵

As in Algorithm 1, the update routine of the invaded-cluster algorithm takes as input a 1-cochain $f_t \in C^1(X; \mathbb{Z}_q)$ and passes through a percolation subcomplex P_{t+1} to sample a spin assignment at time $t + 1$.

Algorithm 2 (Plaquette invaded-cluster).

- (1) Let (x_n) be a uniform random shuffling of the plaquettes of X .
- (2) Set $k := 1$, and let the subcomplex P_0 comprise all vertices and edges of X .
- (3) For each $0 < k \leq n$,
 - (a) add x_k to P_{k-1} if $\delta^1 f(x_k) = 0$, and call the new subcomplex P_k ;
 - (b) if P_k has some desired number of giant cycles, set $P_{t+1} := P_k$ and go to (4).
- (4) Uniformly sample f_{t+1} from $Z^1(P_{t+1}; \mathbb{Z}_q)$, and set $t := t + 1$.
- (5) Return to (1) unless a suitable convergence threshold is met.

Like the invaded-cluster algorithm for the Potts model, we do not have a rigorous proof that this algorithm targets a distribution that converges to Potts lattice gauge theory as $N \rightarrow \infty$. However, the same heuristic described in [28] suggests that this is the case.

4 Sampling via duality

Potts lattice gauge theory is dual to the Potts model on \mathbb{Z}^3 and is self-dual on \mathbb{Z}^4 , relationships classically derived by manipulating partition functions via Fourier expansion [26, 33]. While this interplay lets us describe a model’s thermodynamics in terms of its dual, it is not immediately clear how to re-wire an algorithm that (e.g.) samples the Potts model on \mathbb{Z}^3 to instead sample its dual Potts lattice gauge theory. The duality transformation for the plaquette random-cluster model, however, allows sampling via duality as it is defined explicitly on the probability space.

The *dual lattice* $(\mathbb{Z}^d)^\bullet$ translates every cell of \mathbb{Z}^d by $1/2$ in each coordinate, so each j -cell $x \in \mathbb{Z}^d$ in-

tersects exactly one $(d - j)$ -cell $x^\bullet \in (\mathbb{Z}^d)^\bullet$ called its *dual cell*. The *dual subcomplex* $X^\bullet \subset (\mathbb{Z}^d)^\bullet$ of an i -dimensional subcomplex $X \subset \mathbb{Z}^d$ then comprises dual cells $x^\bullet \in X^\bullet$ if and only if $x \notin X$. If X is distributed as the PRCM with parameters p and q , then X^\bullet is distributed as the PRCM with parameters

$$p^*(p, q) := \frac{(1 - p)q}{(1 - p)q + p}$$

and q .⁶ To make this correspondence precise, we need to take boundary conditions into account: free boundary conditions in the plaquette random-cluster model correspond to wired boundary conditions for the dual [13]. The dual of the PRCM with periodic boundary conditions (that is, on \mathbb{T}_N^d) is “almost” a PRCM with periodic boundary conditions, but needs to be reweighted by a term counting the number of giant cycles in P to obtain an exact duality.⁷ This reweighting disappears in the thermodynamic limit.

Equipped with a duality transformation, we can now sample Potts lattice gauge theory with parameters β and q on (say) a cube in \mathbb{Z}^3 . First, sample the Potts model g on the cube with parameters $\beta^*(\beta, q) = \log(e^\beta + q - 1/e^\beta - 1)$ and q (under appropriate boundary conditions) via any known technique. Next, let P^\bullet be the graph containing each edge e of $(\mathbb{Z}^d)^\bullet$, where $\delta^0 g(e) = 0$ independently with probability $p^*(p, q)$. This way, P^\bullet is distributed as the classical random-cluster model, so its dual P is distributed as the PRCM. Finally, select a cocycle $f \in Z^1(P; \mathbb{Z}_q)$ at uniform random to sample PLGT.

Does the Swendsen–Wang algorithm exhibit the same dynamics as its corresponding procedure on the dual complex? To see that it does not, suppose $P_0 \subset \mathbb{T}_N^3$ contains every 2-cell: any uniform cocycle $f_1 \in Z^1(P_0; \mathbb{Z}_q)$ then vanishes on every 2-cell of the torus, so P_1 is distributed as independent plaquette percolation with probability p . On the other hand, $Q_0 := P_0^\bullet$ is the empty graph containing every vertex of $(\mathbb{T}_N^3)^\bullet$ but none of its edges. As such, $Z^0(Q_0; \mathbb{Z}_q) = C^0(Q_0; \mathbb{Z}_q)$, and a uniform cocycle g_0 on Q_0 assigns a uniformly random spin in \mathbb{Z}_q to each vertex of $(\mathbb{T}_N^3)^\bullet$. After performing one step of Swendsen–Wang dynamics, the probability that a given edge is contained in Q_1 is $p^*(p, q)/q$, and the probability that a dual plaquette is included in Q_1^\bullet is $1 - p^*(p, q)/q \neq p$. Moreover, the states of the plaquettes in Q_1^\bullet are not independent.

Sampling the classical random cluster model on \mathbb{Z}^3 via the Swendsen–Wang dynamics on the dual plaque-

⁵ See Theorem 5 of [12] and Theorem 10 of [14].

⁶ This was first observed in [12]; see Theorem 14 of [13] for the most general statement.

⁷ See the discussion before Theorem 18 of [14].

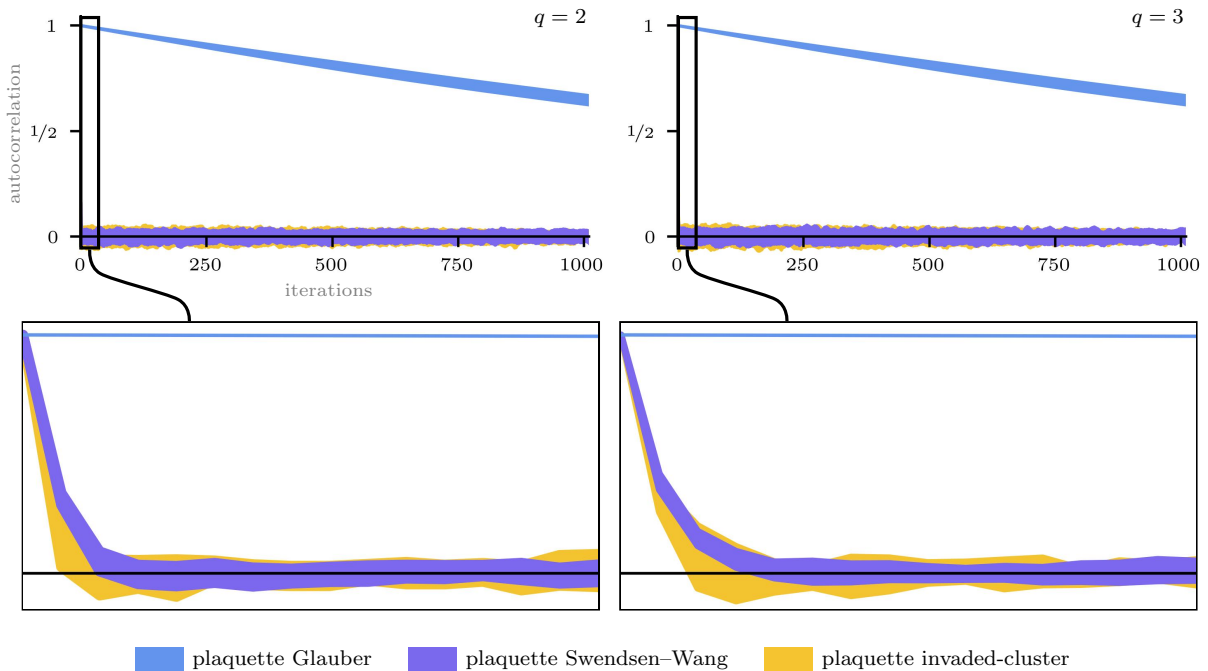


Figure 3: Comparing normalized autocorrelation of energies $\mathbf{H}(f_t)$ for the plaquette Glauber, Swendsen-Wang, and invaded-cluster algorithms on the cubical four-torus \mathbb{T}_{10}^4 for $q = 2$ (left) and $q = 3$ (right) at the self-dual point p_{sd} . Data are shown as fenced regions: for example, all data from the Swendsen-Wang algorithm fall within the purple regions. Top row: autocorrelation truncated to $t = 1000$ iterations. Bottom row: autocorrelation truncated to $t = 15$ iterations. We will continue to update this figure with data from larger simulations.

the random cluster model turns out to be equivalent to sampling from the Loop-Cluster coupling defined in [34]. We further discuss this fact, and an extension to the generalized i -dimensional PRCM (where sampling via duality recovers the generalized Loop-Cluster coupling defined in [22]), in Appendix A.2.

5 Computation and experiments

5.1 Programmatic implementation

To use the most efficient algorithms, we narrow our scope to the cases where q is prime, making \mathbb{Z}_q a field and the cochain group $C^1(X; \mathbb{Z}_q)$ a vector space. Further, the boundary and coboundary operators are linear, so we can describe them exactly by matrices with entries in \mathbb{Z}_q . The i^{th} coboundary matrix δ^i has a row for each i -cell Y and a column for each $(i-1)$ cell Z ; the corresponding entries in δ^i are

$$= \begin{cases} 1 & y \in \partial Z \\ -1 & -y \in \partial Z \\ 0 & \text{otherwise.} \end{cases}$$

As an example, the entries of δ^1 for the edges $\{ab\}$ and $\{ac\}$ of the plaquette $x = \{abcd\}$ in Figure 1 are 1 and -1 , respectively.

With this setup, sampling cocycles f from $C^1(P; \mathbb{Z}_q)$

becomes an exercise in matrix reduction.⁸ We use conjugate Lanczos iteration (as implemented in the LinBox finite-field linear algebra suite [21]) to solve for a uniform random solution to $\delta^1 f = 0$ in step (3) of Algorithm 1 and step (4) of Algorithm 2.

To determine whether we have homologically percolated sufficiently many times — that is, to verify the condition in step (3b) of Algorithm 2 — we use *persistent homology*, which identifies topological features of P that are also topological features of X . We first break X into a nested sequence of subcomplexes called a *filtration*: the first t elements of the filtration are the subcomplexes P_t specified by Algorithm 2, and the remaining elements are the subcomplexes formed by adding each plaquette *not* in P to P_t one at a time.

At each step of the filtration, we then ask whether the added plaquette creates a new cycle or annihilates an existing one — the cycles created at or before time t minus the cycles annihilated after time t are the giant cycles in P , and form the *first persistent homology group* $PH_1(P)$. Computationally, computing (the rank of) this group amounts to re-ordering the columns of the boundary matrices, then reducing to *Smith normal form* [15, 35]. Algorithms 1 and 2, alongside supporting arithmetic and topological rou-

⁸ These matrices are, even for relatively small N , extremely large and sparse: the matrix δ^1 of \mathbb{T}_{10}^4 has 2.4×10^9 entries — of which 8×10^5 are nonzero — for a density of $\approx 0.003\%$.

tines, are implemented in *Algebraic Topology-Enabled Algorithms for Spin systems* (ATEAMS), this work’s companion software library [11]; for more, see Appendix B.

5.2 Experiments and results

Experimentally, we restrict our attention to 2-dimensional plaquette percolation on the 4-dimensional torus with coefficients in \mathbb{Z}_q for prime q . In these systems, the critical point is conjectured to be the self-dual point $p_{\text{sd}} = \sqrt{q}/(1 + \sqrt{q})$ [14]. Using our implementations of the plaquette Swendsen–Wang and invaded-cluster algorithms, we compare their performance to each other and to single-spin flip (or *Glauber*) dynamics on \mathbb{T}_{10}^4 , the cubical 4-torus of scale $N = 10$.

We first compare the *autocorrelation decay* of each algorithm, tracking the statistical similarity between energies $\mathbf{H}(f_0)$ and $\mathbf{H}(f_t)$ as t grows. These data, shown in Figure 3, clearly reflect the algorithms’ sampling methodologies: the destructive Swendsen–Wang and invaded-cluster algorithms lose memory of the initial cochain f_0 within ten iterations. Glauber dynamics are eidetic, remembering f_0 for most of the run-time.

It is important to emphasize that the time scale in Figure 3 corresponds to *iterations* of each algorithm, not the clock time it took to complete them. Plaquette Glauber dynamics bears a comparatively light computational load, while the Swendsen–Wang and invaded-cluster algorithms require more time and resources. As Glauber dynamics edits a single entry of the input cochain, it is only memory-constrained by the scale and dimensionality of the ambient lattice. The plaquette Swendsen–Wang and invaded-cluster algorithms, on the other hand, need to solve a large, sparse system of linear equations at each iteration, and so are time- *and* memory-bound by the lattice

parameters. Finally, the invaded-cluster algorithm’s behavior hews closely to Swendsen–Wang’s at criticality. This differs from the observed behavior of these algorithms for the Potts model, but may be an artifact of the system size. Performance statistics for each model are included in Appendix B.2.

Second, we consider the effect of the topological stopping rule for the plaquette invaded-cluster algorithm. By duality, the probability that the PRCM (sampled at the self-dual point) has at least one giant cycle exceeds $1/2$. As a consequence of Theorem 5, we know that as $N \rightarrow \infty$ the PRCM has — with high probability — no giant cycles when $p < p_{\text{sd}}$, and a full linearly independent set of $\binom{4}{2} = 6$ giant cycles when $p > p_{\text{sd}}$. However, we have no *a priori* prediction for the distribution of the number of giant cycles at p_{sd} besides knowing that it is symmetric and centered about 3. Figure 4 shows the mean percentage of non-frustrated plaquettes included in P_{t+1} before encountering the j^{th} linearly independent giant cycle (for $1 \leq j \leq 6$). This quantity is closest to p_{sd} for $j = 3$ and, as the scale of the torus is taken to infinity, we expect all of these curves to converge to p_{sd} . We conjecture further that the local statistics of sampled plaquette percolations (and coupled spin assignments) will approach those of the self-dual PRCM (and PLGT) for any stopping rule, but a gap remains for $N = 10$.

6 Discussion and conclusions

Using tools borrowed from algebraic topology, we describe versions of the *Swendsen–Wang* and *invaded-cluster* algorithms for targeting q -state Potts lattice gauge theory and the *plaquette random-cluster measure* on cubical tori of arbitrary dimension [6, 14, 28]. These generalized procedures — the *plaquette Swendsen–Wang* and *plaquette invaded-cluster* algorithms (Algorithms 1 and 2) — rely on basic linear

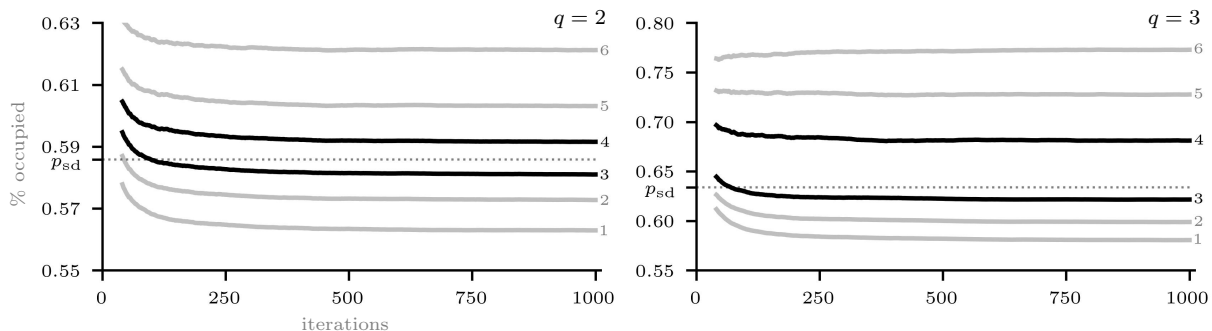


Figure 4: Percentages of non-frustrated plaquettes included in P_{t+1} (occupancy) plotted against iterations of the plaquette invaded-cluster algorithm on the cubical 4-torus \mathbb{T}_{10}^4 for $q = 2$ (left) and $q = 3$ (right) at p_{sd} , amortized over ten simulations. Each curve is annotated the number of linearly independent giant cycles encountered. Dark curves indicate number of giant cycles found before re-sampling f_t ; dotted line indicates the theoretical critical probability $p_{\text{sd}} = \sqrt{q}/(1 + \sqrt{q})$. At each iteration of this experiment (i.e. for each execution of Algorithm 2), we flip a fair coin to decide whether to re-sample f_t after the third or fourth giant cycle is encountered. We will continue to update this figure with data from larger simulations.

algebra and probability. We prove that the plaquette Swendsen–Wang algorithm targets Potts lattice gauge theory, and conjecture that the stationary distribution of the plaquette invaded-cluster algorithm converges weakly to Potts lattice gauge theory in the infinite-volume limit. Further, we empirically demonstrate that the plaquette invaded-cluster algorithm obeys the scaling behavior theorized in [14], showing the algorithm’s efficacy in estimating percolation thresholds for each axis of a given system.

Each algorithm is implemented in ATEAMS [11]. We detail the memory-efficient data structures and subroutines underlying the computational simulations, and believe the implementation to be a robust experimental tool for studying spin systems. In future work, we plan to: further optimize ATEAMS; gather experimental data regarding the scaling behavior of PLGT and PRCM at criticality; estimate the dynamical critical exponents of the plaquette Swendsen–Wang and invaded-cluster algorithms; and use the plaquette invaded-cluster algorithm to estimate homological percolation thresholds in higher-dimensional settings.

Acknowledgements

Anthony E. Pizzimenti was generously supported by the NSF Graduate Research Fellowship Program (#2024370283). The authors are grateful to Summer Eldridge for her contributions to (and testing of) ATEAMS, and to Ramgopal Agrawal, Madeline Horton, and Shrunal Pothagoni for their thoughtful comments on the form and content of this work.

References

- [1] Ramgopal Agrawal et al. “The geometric phase transition of the three-dimensional \mathbb{Z}_2 lattice gauge model”. In: *arXiv preprint arXiv:2409.15123* (2024).
- [2] Michael Aizenman and Jürg Fröhlich. “Topological anomalies in the n -dependence of the n -states Potts lattice gauge theory”. In: *Nuclear Physics B* 235.1 (1984), pp. 1–18.
- [3] Ulrich Bauer et al. “PHAT — Persistent Homology Algorithms Toolbox”. In: *Journal of Symbolic Computation* 78 (Jan. 2017), 76–90. DOI: 10.1016/j.jsc.2016.03.008.
- [4] R Ben-Av et al. “Critical acceleration of Monte-Carlo simulations of $\mathbb{Z}(2)$ gauge theory”. In: *Nuclear Physics B-Proceedings Supplements* 17 (1990), pp. 285–288.
- [5] Omer Bobrowski and Primoz Skraba. “Homological percolation and the Euler characteristic”. In: *Physical Review E* 101.3 (Mar. 2020). DOI: 10.1103/PhysRevE.101.032304.
- [6] Omer Bobrowski and Primoz Skraba. “Homological Percolation: The Formation of Giant k-Cycles”. In: *International Mathematics Research Notices* 2022.8 (Apr. 2022). DOI: 10.1093/imrn/rnaa305.
- [7] Richard C Brower, Suzhou Huang, and Kevin JM Moriarty. “Plaquette percolation for lattice gauge theory”. In: *Nuclear Physics B-Proceedings Supplements* 17 (1990), pp. 603–606.
- [8] Chao Chen and Michael Kerber. “Persistent homology computation with a twist”. In: *Proceedings 27th European workshop on computational geometry*. Vol. 11. 2011, pp. 197–200.
- [9] Michael Creutz, Laurence Jacobs, and Claudio Rebbi. “Experiments with a gauge-invariant Ising system”. In: *Physical Review Letters* 42.21 (1979), p. 1390.
- [10] K Drühl and H Wagner. “Algebraic formulation of duality transformations for abelian lattice models”. In: *Annals of Physics* 141.2 (July 1982), 225–253. DOI: 10.1016/0003-4916(82)90286-X.
- [11] Paul Duncan, Anthony E. Pizzimenti, and Benjamin Schweinhart. *ATEAMS: Algebraic Topology-Enabled Algorithms for Spin systems*. Version 2.0.1. DOI: 10.5281/zenodo.14284172. URL: <https://github.com/apizzimenti/ATEAMS>.
- [12] Paul Duncan and Benjamin Schweinhart. “A Sharp Deconfinement Transition for Potts Lattice Gauge Theory in Codimension Two”. In: *Communications in Mathematical Physics* (2025). URL: <http://arxiv.org/abs/2308.07534>.
- [13] Paul Duncan and Benjamin Schweinhart. *Some Properties of the Plaquette Random-Cluster Model*. June 2024. URL: arxiv.org/abs/10.48550/arXiv.2406.08043.
- [14] Paul Duncan and Benjamin Schweinhart. “Topological Phases in the Plaquette Random-Cluster Model and Potts Lattice Gauge Theory”. In: *Communications in Mathematical Physics* (2025). URL: arxiv.org/abs/10.48550/arXiv.2207.08339.
- [15] Herbert Edelsbrunner and John Harer. *Computational Topology: An Introduction*. American Mathematical Soc., 2010. ISBN: 978-0-8218-4925-5.
- [16] Robert G. Edwards and Alan D. Sokal. “Generalization of the Fortuin-Kasteleyn-Swendsen-Wang representation and Monte Carlo algorithm”. In: *Physical Review D* 38.6 (Sept. 1988), 2009–2012. DOI: 10.1103/PhysRevD.38.2009.

[17] C. M. Fortuin and P. W. Kasteleyn. “On the random-cluster model: I. Introduction and relation to other models”. In: *Physica* 57.4 (Feb. 1972). DOI: 10.1016/0031-8914(72)90045-6.

[18] Paul Ginsparg, Yadin Y Goldschmidt, and Jean-Bernard Zuber. “Large q expansions for q -state gauge-matter Potts models in Lagrangian form”. In: *Nuclear Physics B* 170.3 (1980), pp. 409–432.

[19] Geoffrey Grimmett. *The Random-Cluster Model*. Ed. by Harry Kesten. Springer Berlin Heidelberg, 2004. ISBN: 978-3-662-09444-0. DOI: 10.1007/978-3-662-09444-0_2.

[20] The LinBox group. *Givaro*. v4.2.1. 2025. URL: <https://github.com/linbox-team/givaro>.

[21] The LinBox group. *LinBox*. v1.7.0. 2021. URL: <http://github.com/linbox-team/linbox>.

[22] Ulrik Thinggaard Hansen, Jianping Jiang, and Frederik Ravn Klausen. “A General Coupling for Ising Models and Beyond”. In: *arXiv preprint arXiv:2506.10765* (2025).

[23] Allen Hatcher. *Algebraic Topology*. Cambridge University Press, 2002. ISBN: 978-0-521-79540-1.

[24] Yasuaki Hiraoka and Tomoyuki Shirai. “Tutte polynomials and random-cluster models in Bernoulli cell complexes (Stochastic Analysis on Large Scale Interacting Systems)”. In: *RIMS Kokyuroku Bessatsu* B59 (July 2016), 289–304.

[25] Tomasz Kaczynski, Konstantin Mischaikow, and Marian Mrozek. *Computational Homology*. Vol. 157. Applied Mathematical Sciences. Springer, 2004. ISBN: 978-1-4419-2354-7.

[26] John B. Kogut. “An introduction to lattice gauge theory and spin systems”. In: *Reviews of Modern Physics* 51.4 (Oct. 1979), 659–713. DOI: 10.1103/RevModPhys.51.659.

[27] J. Machta et al. “Invaded Cluster Algorithm for Equilibrium Critical Points”. In: *Physical Review Letters* 75.15 (Oct. 1995), 2792–2795. DOI: 10.1103/PhysRevLett.75.2792.

[28] J. Machta et al. “Invaded cluster algorithm for Potts models”. In: *Physical Review E* 54.2 (Aug. 1996). DOI: 10.1103/PhysRevE.54.1332.

[29] A Maritan and C Omero. “On the gauge Potts model and the plaquette percolation problem”. In: *Nuclear Physics B* 210.4 (1982), pp. 553–566.

[30] Peter Saveliev. *Topology Illustrated*. Independent Publisher, Feb. 2016. ISBN: 978-1-08-780346-3.

[31] Yakov Shklarov. “The Edwards-Sokal Coupling for the Potts Higher Lattice Gauge Theory on \mathbb{Z}^d ”. MA thesis. The University of Victoria, 2023.

[32] Robert H. Swendsen and Jian-Sheng Wang. “Nonuniversal critical dynamics in Monte Carlo

simulations”. In: *Physical Review Letters* 58.2 (Jan. 1987). DOI: 10.1103/PhysRevLett.58.86.

[33] Franz J. Wegner. *Duality in generalized Ising models*. Nov. 2014. DOI: 10.48550/arXiv.1411.5815. URL: <http://arxiv.org/abs/1411.5815>.

[34] Lei Zhang et al. “Loop-cluster coupling and algorithm for classical statistical models”. In: *Physical Review Letters* 125.20 (2020), p. 200603.

[35] Afra J. Zomorodian. *Topology for Computing*. Cambridge University Press, 2005. ISBN: 978-0-521-83666-1.

A Definitions

A.1 Algebraic topology

Let e_i denote the line segment between the origin in \mathbb{Z}^d and the endpoint of the vector \vec{e}_i (for $1 \leq i \leq d$). The set $\mathcal{D} = \prod e_i$ is then a unit d -cube (or d -cell).

To convert geometry to algebra, we treat point-set topological boundaries as finite linear combinations of the faces composing them: the set $C_i(X, G)$ is the i^{th} chain group of the cubical complex X with coefficients in the abelian group G . An i -chain in $C_i(X, G)$ is a linear combination

$$\gamma = \sum \alpha_j x_j,$$

where the α_j are in G and the x_j i -cells of X . The i^{th} boundary map $\partial_i : C_i(X, G) \rightarrow C_{i-1}(X, G)$ takes an i -cell x to an oriented sum of its faces. Ordering the set $F = (F_1, \dots, F_n)$ of x 's faces lexicographically by their vertex coordinates, the boundary of x is

$$\partial_i(x) = \sum_{k=1} (-1)^{k-1} F_k.$$

Figure 5 demonstrates ∂_2 when applied to a 2-cube (or *square plaquette*) — edges are always oriented to “point” from the lesser to the greater coordinate, so the boundary of the square is the alternating sum over its edges in lexicographic order.⁹ Moreover, the boundary maps are homomorphisms: given an i -chain $\gamma = \sum \alpha_j x_j$,

$$\begin{aligned} \partial_i(\gamma) &= \partial_i \left(\sum \alpha_j x_j \right) \\ &= \sum \alpha_j \partial_i(x_j). \end{aligned}$$

These maps also satisfy the relation $\partial_{i-1}\partial_i = 0$ for all i (where $\partial_0 = 0$), as shown in Figure 5. All told, we have a *chain complex*

$$C_i(X, G) \xrightarrow{\partial_i} C_{i-1}(X, G) \xrightarrow{\partial_{i-1}} \dots \xrightarrow{\partial_1} C_0(X, G) \xrightarrow{\partial_0} 0,$$

⁹ The face ordering is arbitrary so long as the $\partial_{i-1}\partial_i = 0$ condition is satisfied. We choose lexicographic order for its relative simplicity, ease of computation, and precedent in relevant literature [10].

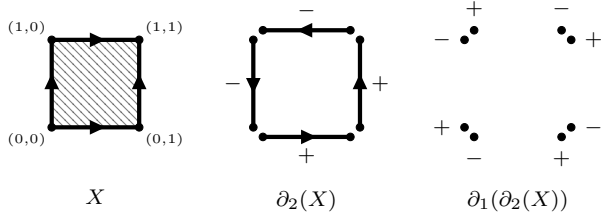


Figure 5: For X the unit 2-cube $e_1 \times e_2$ (left, with vertices labeled): X 's bounding 1-chain (center); the bounding 0-chain of X 's bounding 1-chain (right).

a sequence of abelian groups connected by their respective boundary maps. Because the composition of consecutive boundary maps is zero, we know that $\text{im}(\partial_{i+1}) \subseteq \ker(\partial_i)$ — where the chains in $\text{im}(\partial_{i+1})$ are called *boundaries* and those in $\ker(\partial_i)$ called *cycles* — and so define the i^{th} cubical homology group with coefficients in G as the quotient group $H_i(X, G) := \ker(\partial_i) / \text{im}(\partial_{i+1})$. When $G = \mathbb{F}$ is a field (as is the case in the computational experiments), the $H_i(X, \mathbb{F})$ are vector spaces over \mathbb{F} . Moreover, when X is finite, the boundary operators ∂_i can be represented as matrices with entries in \mathbb{F} [15, 23, 25, 30].

Cochains play the dual role to chains: the i^{th} cochain group with coefficients in G is $C^i(X; G) := \text{Hom}(C_i(X, G), G)$, the group of homomorphisms from the i^{th} chain group into G . The i^{th} coboundary operator δ^i takes an i -cochain f to an $(i+1)$ -cochain by evaluating f on boundaries of $(i+1)$ -chains. Given an $(i+1)$ -chain γ , we set

$$(\delta^i f)(\gamma) := f(\partial_{i+1}(\gamma)),$$

so the composition $f\partial_{i+1}$ is an $(i+1)$ -cochain. We get a dual cochain complex

$$C^{i+1}(X; G) \xleftarrow{\delta^{i+1}} C^i(X; G) \xleftarrow{\delta^i} \dots \xleftarrow{\delta^0} C^0(X; G) \xleftarrow{0} 0$$

connecting the cohomology groups by coboundary maps with the property that $\delta^{i+1}\delta^i = 0$. The i^{th} cubical cohomology group with coefficients in G is the quotient group $H^i(X; G) := \ker(\delta^{i+1}) / \text{im}(\delta^i)$. A consequence of the *universal coefficient theorem for cohomology* tells us that $H_i(X, G) \cong H^i(X; G)$ when G is a field and $H_i(X, G)$ is *finitely generated*. As with boundary operators, the coboundary operators δ^i can be represented as matrices with entries in \mathbb{F} when X is finite; because the boundary and coboundary operators are exact duals under these conditions, $\delta^{i-1} = \partial_i^\top$ [23, 30].

Given a subcomplex $Q \subseteq X$, inclusion $\iota : Q \hookrightarrow X$ induces a map $\iota^* : H_i(Q) \rightarrow H_i(X)$ on homology. More formally, the map ι^* takes equivalence classes of i -chains in Q to equivalence classes of i -chains in X , and classes $[\gamma] \in H_1(Q)$ are nonzero in $H_1(X)$ only when γ does not bound an $(i+1)$ -chain in Q or in

X . The image of ι^* is the i^{th} persistent homology group $PH_i(Q) := \text{im}(\iota^*)$ [15, 35]. In the parlance of homological percolation, these persistent i -cycles are *giant* or *essential* cycles, and are present whenever ι^* is not the zero map [5, 6]. For our purposes, X is typically the scale- N d -fold torus \mathbb{T}_N^d .

A.2 Hyperlattice gauge theory

We can extend the random-cluster and Potts measures to ones on subcomplexes of arbitrary dimension. The $(i-1)$ -dimensional Potts (hyper)lattice gauge theory ν on a finite cubical complex X with parameters $p = 1 - e^{-\beta}$ and integer q is the Gibbs distribution on $C^{i-1}(X; \mathbb{Z}_q)$ induced by the Hamiltonian

$$\mathbf{H}(f) = - \sum_{x \in X} \mathbf{1}_{(\delta^{i-1}f)(x)=0},$$

where $f \in C^{i-1}(X; \mathbb{Z}_q)$, and x are i -cells of X . Thus,

$$\nu(f) = \frac{1}{\mathcal{Z}} e^{-\beta \mathbf{H}(f)},$$

where \mathcal{Z} is the normalizing constant

$$\mathcal{Z} = \sum_{f^*} e^{-\beta \mathbf{H}(f^*)},$$

summing over all $(i-1)$ -cochains f^* .

For a finite cubical complex X , the i -dimensional plaquette random-cluster measure μ with parameters $p \in [0, 1]$ and integer q is the probability distribution

$$\mu(P) = \frac{1}{\mathbf{Q}} p^{|P|} (1-p)^{|X|-|P|} |H^{i-1}(P; \mathbb{Z}_q)|$$

over i -subcomplexes $P \subseteq X$ that contain all cells of dimension $(i-1)$ or lower. The normalizing constant \mathbf{Q} is

$$\mathbf{Q} = \sum_{P^*} p^{|P^*|} (1-p)^{|X|-|P^*|} |H^{i-1}(P^*; \mathbb{Z}_q)|$$

summing over all i -subcomplexes $P^* \subseteq X$ containing all cells of dimension $(i-1)$ or lower. When q is prime, we can re-define the distribution and normalizing constant to

$$\mu(P) = \frac{1}{\mathbf{Q}} p^{|P|} (1-p)^{|X|-|P|} q^{\mathbf{b}_{i-1}(P)}$$

and

$$\mathbf{Q} = \sum_{P^*} p^{|P^*|} (1-p)^{|X|-|P^*|} q^{\mathbf{b}_{i-1}(P^*)},$$

where

$$\mathbf{b}_{i-1}(Q) = \text{rank}(H_{i-1}(Q, \mathbb{Z}_q))$$

is the i^{th} Betti number of $Q \subseteq X$. [12, 24]

The plaquette Swendsen–Wang and plaquette invaded cluster algorithms immediately generalize to these systems. The i -dimensional PRCM also satisfies a duality property: if P is distributed as the i -dimensional PRCM with parameters p and q , then the dual complex P^\bullet obtained by including cells in $(\mathbb{Z}^d)^\bullet$ that do *not* intersect a cell of P is a $(d-i)$ -dimensional PRCM with parameters

$$p^\bullet(p, q) = \frac{p}{p + q(1 - p)}$$

and q after boundary conditions are correctly accounted for. See [13] for a precise statement.

Continuing the discussion of Section 4, suppose that P is distributed as the i -dimensional PRCM. The distribution of P is unchanged by the following operation:

- (1) Let P^\bullet be the dual complex of P .
- (2) Sample a uniform random cocycle f from $Z^{d-i-1}(P^\bullet; \mathbb{Z}_q)$.
- (3) Let P_{new}^\bullet include the dual $(d-i)$ -faces on which $\delta^{i-1}f$ vanishes independently with probability $p^\bullet(p, q)$.
- (4) Let P_{new} be the dual complex of P_{new}^\bullet .

To restate this operation without duality, we use the *discrete Hodge star operator*

$$* : C^{d-i-1}((\mathbb{Z}^d)^\bullet; \mathbb{Z}_q) \rightarrow C_{i+1}(\mathbb{Z}^d; \mathbb{Z}_q).$$

Towards that end, let $\sigma^\bullet \in (\mathbb{Z}^d)^\bullet$ be the $(d-i-1)$ -cell dual to the $(i+1)$ -cell $\sigma \in \mathbb{Z}^d$, and define $f_{\sigma^\bullet} \in C^{d-i-1}((\mathbb{Z}^d)^\bullet; \mathbb{Z}_q)$ by setting $f_{\sigma^\bullet}(\sigma) = \mathbf{1}_{\sigma=\sigma^\bullet}$ and extending linearly. The $*$ operator is the linear extension of the map $f_{\sigma^\bullet} \mapsto \sigma$, where $\partial * = * \delta$.

Now, if f is a uniformly random element of $Z^{d-i-1}(P^\bullet; \mathbb{Z}_q)$, the previous identity implies that $\partial * f$ is an i -cycle supported on P . Assuming the underlying complex is simply connected, this cycle is a uniform random element of $Z_i(P; \mathbb{Z}_q)$. Putting everything together, the i -cells of P_{new} are found by starting with the *trace* of this uniform random i -cycle — the set of i -cells appearing in it with a non-zero coefficient — and adding additional i -cells independently with probability $p^\bullet(p, q)$. In all, we have sampled the PRCM via the generalized Loop–Cluster coupling defined in Section 4 of [22].

B ATEAMS

ATEAMS is an open-source library written in C++, Cython, and Python. It implements Algorithm 1, Algorithm 2, and Glauber dynamics in the `SwendsenWang`, `InvadedCluster`, and `Glauber` classes, respectively. ATEAMS also provides narrow Python bindings to `LinBox`. All matrices are stored in COO (“coordinate-list”) format, and so require space linear in the number of cells; these matrices are tied to a `Cubical` complex object that can be written to and read from a compressed file format for re-use by any of the models above. To give a sense of these objects’ sizes, a `Cubical` instance representing \mathbb{T}_{40}^4 is $\approx 1.3\text{GB}$ when compressed but requires $\approx 20\text{GB}$ of working memory, as the full boundary matrix for \mathbb{T}_{40}^4 has 40,960,000 columns and 166,400,000 nonzero entries.

B.1 Computing persistence

In general, persistent homology is computed with respect to the *full boundary matrix* of a complex X — that is, the matrix ∂ with a row and column for every cell of every dimension, and ± 1 in position (i, j) when cell i is a face of cell j [15]. Filtrations are thus equivalent to a permutation of columns in ∂ . The `twist_reduce` algorithm in PHAT [3, 8] proceeds by scanning through the columns of ∂ in descending order of dimension, setting columns to zero whenever they correspond to cells of a homology class annihilated by some higher-dimensional cell. The magic of PHAT, however, lies in its representation of boundary matrices: since the value of a nonzero entry over \mathbb{Z}_2 is always 1, only the *indices* of these entries are ever stored.

When computing persistence over \mathbb{Z}_q for $q = 2$, we use PHAT; otherwise, we have to keep track of both the indices *and* values of nonzero entries in ∂ . We follow PHAT’s lead in ATEAMS, representing ∂ as a C++ standard `vector` of `map<int, char>`s, where each `map` represents a column of ∂ . C++ standard `maps` are *red-black trees*, which allow us to look up the largest-indexed entry of each column in $O(\log n)$ time. We adopt the column-reduction and -marking strategy of Algorithm `REDUCEPIVOTROWS` in Section 7.3 of [35], which extends `twist_reduce` to operate over a finite field. In ATEAMS, the `Twist` object implements three variants of the modified `twist_reduce`, each with a different mode of arithmetic: `Twist.Compute` uses 2D `char` arrays to store addition and multiplication tables; `Twist.ZpCompute` uses Givaro, a `LinBox` product [20]; `Twist.LinearCompute` uses 1D `char` arrays with modified indexing. In the short run, `Twist.LinearCompute` is $\approx 25\%$ faster than the other methods.

B.2 Performance

Below are performance statistics for various configurations of the `SwendsenWang` and `InvadedCluster` models. We perform 100 iterations of each configuration on Pangolin, a Dell Precision 5280 workstation with an 18-core Intel Xeon W-2295 processor clocked at 1.3GHz. We will continue to update the tables with data from larger simulations. The columns are:

Field	The finite field over which computations were performed.
N	Scale (side length) of the torus \mathbb{T}_N^d .
Plaq	The total number of plaquettes in \mathbb{T}_N^d ; equivalently, the maximum number of rows in $\delta^{(d/2)-1}$.
Cells	The total number of cells in the complex (if applicable); equivalently, the number of columns in the full boundary matrix ∂ .
Tries	The maximum number of times the kernel sampler is allowed to attempt the cocycle-finding computation (if kernel-sampling is a component of the model’s proposal scheme).
s/it	Seconds per iteration.

`SwendsenWang`’s speed modestly increases with q , as `LinBox` tends to handle fields of larger characteristic more quickly. Moreover, the model is generally robust to increases in scale or re-samples allowed: the slowest recorded configuration of `SwendsenWang` takes ≈ 8 seconds per iteration when allowed 32 **Tries** on \mathbb{T}_{30}^4 with coefficients in \mathbb{Z}_2 . Most issues arise when the `Cubical` instance is too big. In practicality, experiments with `SwendsenWang` are efficient and easily performed on a laptop computer.

When $N = 10$, PHAT allows for fast computation over \mathbb{Z}_2 ; `InvadedCluster` is (curiously, prohibitively) slow for $q = 3$ but faster for $q > 3$. Repeated tests suggest that `InvadedCluster` is sensitive to initial conditions, or has an as-yet undiscovered performance sink. Further, as persistence is computed with the full boundary matrix, `InvadedCluster`’s performance deteriorates rapidly with increases in N .

B.3 Swendsen–Wang

Performance in \mathbb{T}_N^2 .

Field	N	Plaq	s/it	
			Tries	
\mathbb{Z}_2	724	1,048,352	8	0.460
			16	0.948
			32	1.519
	1024	2,097,152	8	0.966
			16	1.478
			32	2.316
	1448	4,193,408	8	2.112
			16	4.273
			32	6.383
\mathbb{Z}_3	724	1,048,352	8	0.361
			16	0.345
			32	0.419
	1024	2,097,152	8	0.716
			16	0.825
			32	1.161
	1448	4,193,408	8	1.483
			16	1.496
			32	1.610
\mathbb{Z}_5	724	1,048,352	8	0.239
			16	0.279
			32	0.363
	1024	2,097,152	8	0.537
			16	0.473
			32	0.814
	1448	4,193,408	8	1.472
			16	1.307
			32	1.270
\mathbb{Z}_7	724	1,048,352	8	0.196
			16	0.256
			32	0.225
	1024	2,097,152	8	0.533
			16	0.507
			32	0.463
	1448	4,193,408	8	1.240
			16	1.267
			32	1.181

Performance in \mathbb{T}_N^4 .

Field	N	Plaq	s/it	
			Tries	
\mathbb{Z}_2	10	60,000	8	0.030
			16	0.048
			32	0.104
	20	960,000	8	0.670
			16	0.955
			32	1.375
	30	4,860,000	8	3.772
			16	6.237
			32	8.235
\mathbb{Z}_3	10	60,000	8	0.020
			16	0.026
			32	0.037
	20	960,000	8	0.497
			16	0.487
			32	0.581
	30	4,860,000	8	3.087
			16	3.051
			32	3.698
\mathbb{Z}_5	10	60,000	8	0.016
			16	0.016
			32	0.016
	20	960,000	8	0.327
			16	0.339
			32	0.333
	30	4,860,000	8	2.827
			16	2.730
			32	3.506
\mathbb{Z}_7	10	60,000	8	0.016
			16	0.015
			32	0.015
	20	960,000	8	0.319
			16	0.322
			32	0.309
	30	4,860,000	8	2.987
			16	2.823
			32	3.150

B.4 Invaded-cluster

Performance in \mathbb{T}_N^2 .

Field	N	Cells	Tries	s/it
\mathbb{Z}_2	128	65,536	8	0.042
			16	0.041
			32	0.042
	181	131,044	8	0.094
			16	0.093
			32	0.094
	256	262,144	8	0.208
			16	0.211
			32	0.208
\mathbb{Z}_3	128	65,536	8	3.010
			16	3.261
			32	3.462
	181	131,044	8	13.182
			16	13.402
			32	13.534
	256	262,144	8	52.350
			16	47.104
			32	49.161
\mathbb{Z}_5	128	65,536	8	2.673
			16	2.649
			32	2.662
	181	131,044	8	9.569
			16	9.797
			32	9.069
	256	262,144	8	34.302
			16	35.113
			32	34.551
\mathbb{Z}_7	128	65,536	8	2.929
			16	2.888
			32	2.919
	181	131,044	8	9.403
			16	9.312
			32	9.137
	256	262,144	8	31.836
			16	31.583
			32	31.715

Performance in \mathbb{T}_N^4 .

Field	N	Cells	Tries	s/it
\mathbb{Z}_2	10	160,000	8	0.362
			16	0.301
	20	2,560,000	8	157.579
			16	216.076
\mathbb{Z}_3	10	160,000	8	185.233
			16	109.523
\mathbb{Z}_5	10	160,000	8	129.678
			16	30.151
\mathbb{Z}_7	10	160,000	8	93.875
			16	38.129